Soft Matter

Accepted Manuscript

This article can be cited before page numbers have been issued, to do this please use: M. G. Herrera, L. A. Benedini, C. Lonez, P. L. Schilardi, T. Hellweg, J. Ruysschaert and V. I. Dodero, *Soft Matter*, 2015, DOI: 10.1039/C5SM01619C.

View Article Online
DOI: 10.1039/C5SM01619C

Title: Self-assembly of 33-mer gliadin peptide oligomers

Authors: M. G. Herrera[1], L. A. Benedini [1], C. Lonez [2], P.L. Schilardi [3], T. Hellweg [4], J-M Ruysschaert [5] and V. I. Dodero [1,6]*

Affiliation: [1] Departamento de Química-INQUISUR, Universidad Nacional del Su-CONICET, Av. Alem 1253, Bahía Blanca, Argentina. [2]Department of Veterinary Medicine, University of Cambridge, United Kingdom. [3] Instituto de Investigaciones Fisicoquímicas Teóricas y Aplicadas (INIFTA), CONICET – Departamento de Química, Facultad de Ciencias Exactas, UNLP, CC16, Suc. 4(1900) La Plata, Buenos Aires, Argentina.[4] Universität Bielefeld, Fakultät für Chemie, Physikalische und Biophysikalische Chemie, Universitätsstr. 25, 33615 Bielefeld, Germany, [5] Structure and Function of Biological Membranes, Université Libre de Bruxelles, Belgium, [6] Universität Bielefeld, Fakultät für Chemie, Organische Chemie, Universitätsstr. 25, 33615 Bielefeld, Germany.

*To whom correspondence should be addressed.
Prof. Dr. Verónica I. Dodero, María G. Herrera and Luciano A. Benedini
Departamento de Química-INQUISUR
Universidad Nacional del Sur-CONICET. Av. Alem 1253, 8000 Bahía Blanca, Argentina
Tel: +54-291-4595101 ext: 3540, Fax: +54-291-4595187
E-mail: veronica.dodero@uns.edu.ar

Dr. Caroline Lonez
Department of Veterinary Medicine, University of Cambridge, United Kingdom
Madingley Road, CB30ES
Tel: +44 (0)1223 766232, Fax: +44(0)1223 337610
E-mail: cl500@cam.ac.uk

Dr. Jean Marie Ruysschaert
Structure and Function of Biological Membranes, Université Libre de Bruxelles, Belgium
Tel +3226505377, Fax +3226505382,
E-mail: jmruyss@ulb.ac.be

Dr. Patricia Schilardi
Instituto de Investigaciones Fisicoquímicas Teóricas y Aplicadas (INIFTA), CONICET – Departamento de Química, Facultad de Ciencias Exactas, UNLP, La Plata, Buenos Aires, Argentina.
Tel: + 54 221 425 7430 / 7291 Ext. 135, Fax: +54 221 425 4642
E-Mail: pls@inifta.unlp.edu.ar

Prof. Dr. Thomas Hellweg
Bielefeld University, Department of Chemistry
Physical and Biophysical Chemistry (PC III)
Universitätsstr. 25, 33615 Bielefeld
Tel: +49 521-106-6888, Fax: +49 521-106-2981
E-Mail: thomas.hellweg@uni-bielefeld.de

View Article Online
DOI: 10.1039/C5SM01619C

Introduction:

Gluten is a protein complex present in wheat, oat, rye and barley formed by glutenin and gliadin. Gliadin is highly immunogenic [1] and it is not completely digested by humans. After *in vitro* or *in vivo* (murine models) proteolytic degradation, a resistant peptide of 33 amino acids (33-mer), LQLQPF$(PQPQLPY)_3$PQPQPF, remains intact among other smaller peptides. [2] This 33-mer fragment is considered as one of the most important immunological modulator peptides responsible for celiac disease, a complex immunological disorder with a prevalence of 1% among the healthy population. [2, 3] Recently, a new pathology named gluten sensitivity has been described and its prevalence is even higher than celiac disease, estimated as a 7% of the total population. [4] Up to now, the only treatment for both pathologies is a gliadin-free life-long diet. [5]

Although the immunological response observed in the chronic phase of celiac disease is well characterized, the initiation of these inflammatory events is still obscure. [1, 6 7] Regardless the first steps involved in the innate or/and adaptive immunological response, an essential prerequisite could be the initiating role of the digestive-resistant gliadin peptide fragments, such as the 33-mer studied here. Previous work showed that the 33-mer is able to self-assemble into quaternary structures at physiological concentrations. [8] Also, a structural transition was reported during 33-mer concentration dependent self-organization in solution, from an unfolded to a more folded state. Conformational transition and self-association were described for other proteins implicated in diseases such as Alzheimer [9] and Parkinson. [10] In both pathologies, protein oligomers have been associated to an innate and adaptive immune activation. [11, 12] The characterization of 33-mer supramolecular structures could therefore be a first step towards the understanding of the early stages of gliadin intolerance disorders. The aim of this study is to get a better insight into the 33-mer oligomer structure and the relationship between its secondary structure and its self-assembly capacity.

View Article Online
DOI: 10.1039/C5SM01619C

Material and Methods

Sample preparation

The 33-mer gliadin peptide LQLQPF(PQPQLPY)$_3$PQPQPF (3911 Da) (95% purity, lyophilized powder) was purchased from Biochem Shanghai Ltd and characterized by HPLC-ESI and MALDi-ToF. Five different synthetic samples of 33-mer peptide purchased at different periods were employed. Purity and mass integrity were reexamined before and after experiments to ensure that no chemical modification occurred during handling. Samples were prepared with high-purity water from a Milli-Q water purification system (Millipore/Waters) or in some cases from a Satorius water Purification system. Buffer salt concentrations were: 10 mM of sodium citrate, sodium borate, sodium phosphate, and 150 mM of NaCl, pH 7. Both solutions were filtered through a filter of 13 mm of diameter and pore size of 220 nm in a laminar flow bench to avoid the presence of dust particles. Desired concentrations were obtained starting from a high concentration sample taken the correct volume and adding the filtered water or buffer to reach the final concentration. Big clusters were separated from the small oligomers 33-mer gliadin peptide by sample filtration using a 220 nm filter with a Millex Durapore membrane.

Dynamic light scattering (DLS)

DLS experiments were carried out using 3D LS Spectrometer (LS Instruments, Fribourg, Switzerland). The light source was a He-Ne laser operated at a wavelength of 632.8 nm with a constant output power of 30 mW. For more details see ref.[13,14] The scattering experiments were performed with an angular range of $40° > \theta > 110°$. Samples were kept in the thermostatised goniometer of the DLS instrument between 15 to 20 minutes to reach a thermal equilibrium. In order to obtain, a well-defined baseline of the correlation functions, counts were accumulated for 4 to 5 h. for each correlation function. The measured intensity time autocorrelation functions were converted to the respective field correlation functions and analysed using the CONTIN

View Article Online
DOI: 10.1039/C5SM01619C

software of S. Provencher. [15] The latter provided the intensity weighted rate distribution of the formed structures in the samples. This can be easily converted into a distribution of apparent diffusion coefficients. Using the Stokes-Einstein equation one can calculate the radii of hydrodynamically equivalent spheres and these radii are used in the following discussion (see Supplementary Information, SI). Due to the rather complex aggregation behaviour found in the solutions we simplified the results by grouping the hydrodynamic radii calculated from the individual runs into three size categories: ≤ 100, 100-1000 and ≥ of 1000 nm. To avoid preformed aggregates, all samples were filtered immediately prior DLS measurements following the procedure described in sample preparation. Hence, all observed contributions to the decay of the correlation functions corresponding to particles larger than 220 nm arise from dynamical aggregation equilibria in the 33-mer solutions.

Atomic force microscopy (AFM)

Contact mode AFM (Nanoscope V; Bruker, Santa Barbara, CA) was used to characterize the peptide oligomerization using silicon nitride tips (Bruker) (spring constant, 0.12 N/m). Water aqueous solutions of the peptides at concentrations from 6, 60, 250 and 610μM were deposited on freshly cleaved mica, and left to interact with the surface for five minutes at room temperature. Then the samples were dried by a Nitrogen flow. In all cases, the topographic and deflection error channels were used to image the samples. The height and the full width at half-maximum (FWHM) of the observed architectures were determined by cross section using Nanoscope Analysis 1.1 software (Bruker). The FWHM was selected in order to compensate the distortion introduced by the geometry of the tip. [16,17] The coverage was evaluated using Image J software. [18] The volume and radius of the spheres were estimated as described by Tanford et. al. and Pietrasanta et.al. (see SI).

Fractal analysis

View Article Online
DOI: 10.1039/C5SM01619C

Fractal analysis of the AFM images of 33-mer gliadin peptide at concentrations of 6, 60, 250, and 610 μM was performed using Image J.[18] The Box Counting algorithm was used to get the information about fractal properties. The topographic images were transformed to 8-bit binary format and the box values of 4, 8, 16, 32, 64 and 128 were overlaid in the image to obtain the fractal dimension (D_f) of the whole picture (see SI).

Attenuated total reflectance (ATR)-Fourier-transform infrared spectroscopy (FTIR)

IR spectra were recorded at a constant temperature of 21 °C on an Equinox 55 infrared spectrophotometer (Bruker Optics, Ettlingen, Germany) equipped with a Golden Gate reflectance accessory (Specac, Slough, United Kingdom) and a mercury cadmium telluride liquid nitrogen detector. The internal reflection element was a diamond crystal (2×2 mm) with an aperture angle of 45° that yielded a single internal reflection. Each spectrum represents the mean of 128 repetitions (to reduce the signal / noise ratio) which were recorded with *OPUS* software at a resolution of 2 cm^{-1} while the spectrophotometer was continuously purged with dried air. Samples were prepared by spreading 2 μl (~10 ng) of 33-mer peptide oligomers on the diamond crystal surface and by removing the excess water under nitrogen flow, yielding a thin film of peptide sample. Deuteration was obtained by flushing the samples with ^2H_2O- saturated nitrogen stream for at least 45 min. The software used for analysing the spectra was the SFMB-developed Matlab program *KINETICS.*[19] The ATR-FTIR data were processed by subtracting the water vapor contribution with 1562-1555 cm^{-1} as reference peak and spectra were baseline corrected (1792, 1729, 1575 and 1484 cm^{-1}) and smoothed at a final resolution of 4 cm^{-1} by apodization of their Fourier transform by a Gaussian line. Spectral intensities were finally rescaled on the amide I peak area (1729-1575 cm^{-1}) to normalize protein amounts between all measurements. Finally, all spectra were self-deconvoluted using a Lorentzian deconvolution factor with a full width

View Article Online
DOI: 10.1039/C5SM01619C

at half height of 30 cm^{-1} and a Gaussian apodization factor with full width at half height of 15 cm^{-1} to obtain a resolution enhancement factor of 2. Deconvolution increases the resolution of the spectra in the amide I region, which is most sensitive to the secondary structure of proteins.

Results and Discussion

Detection of 33-mer self-assembly in aqueous medium by dynamic light scattering (DLS)

In the present work we used DLS to probe the solution self-assembly of the 33-mer over a broad range of concentrations. In a previous work, it was shown by electron microscopy (EM), that the morphology of the aggregates at 610 µM corresponds to different quaternary structures such as nanospheres (14, 35 and 66 nm of diameter), filaments (28 and 58 nm in width) and fibrils (from 200 to 800 nm in width).[8] In addition, circular dichroism (CD) experiments also indicated that increasing 33-mer peptide concentration from 6 to 610 µM, induced a structural transition accompanied by a self-assembly process. [8] However so far, the size and occurrence of the self-assembled structures could not be characterized. In the present work, all samples were filtered with 220 nm pore filter immediately prior to DLS measurements to avoided preformed aggregates (see Material and methods). The kinetics of 33-mer assembly is fast and metastable soluble aggregates are formed in the whole concentration range. Our DLS measurements showed that in aqueous medium the 33-mer is organized as a poly-disperse system in the 125 to 610 µM concentration range (Figure 1 and Table 1). In the case of multimodal or polydisperse particle size distribution, a regularization approach is the best choice to analyse DLS results. [20] This method assumes that the distribution is an arbitrary, but smooth function, and seeks a non-negative distribution producing the best fit to the experimental observed correlation function. The regularization requirement of smoothness precludes spikes in the distribution, allowing unique solutions to the minimization problem. Several regularization algorithms differ in

View Article Online
DOI: 10.1039/C5SM01619C

the specific mathematical implementation of the smoothness conditions. Here, we used the CONTIN regularization method [15] which employed the standard inverse Laplace transform approach. The outcome is an intensity weighted relaxation rate distribution which can be converted into a distribution of the corresponding hydrodynamic radii of the present structures. CONTIN provides all the relevant moments for the different peaks in the computed distribution function allowing to calculate the mean value for each peak (or relaxation mode) and the standard deviation of that specific peak. Due to the polydispersity of the 33-mer system and to simplify the discussion of the results, the hydrodynamic radii of 33-mer assemblies have been classified into three categories: ≤ 100, 100-1000 and ≥ of 1000 nm. Similar polydisperse distributions were reported in other peptides and self-organizing protein systems, with different globular morphologies. [21-23] In addition, in amyloid systems, high polydispersity was found and explained in terms of metastable oligomers formation in aqueous solution, normally at physiological conditions. [24]

Since the Rayleigh scattering intensity depends on R^6 large particles are dominating the intensity distribution. A volume or particle number weighted distribution can be obtained using a different kernel function. [25] However, this was beyond the scope of the present work and the intensity-weighted approach reveals already the most important information about the distribution of the hydrodynamic radii of 33-mer based particles in solution.

View Article Online
DOI: 10.1039/C5SM01619C

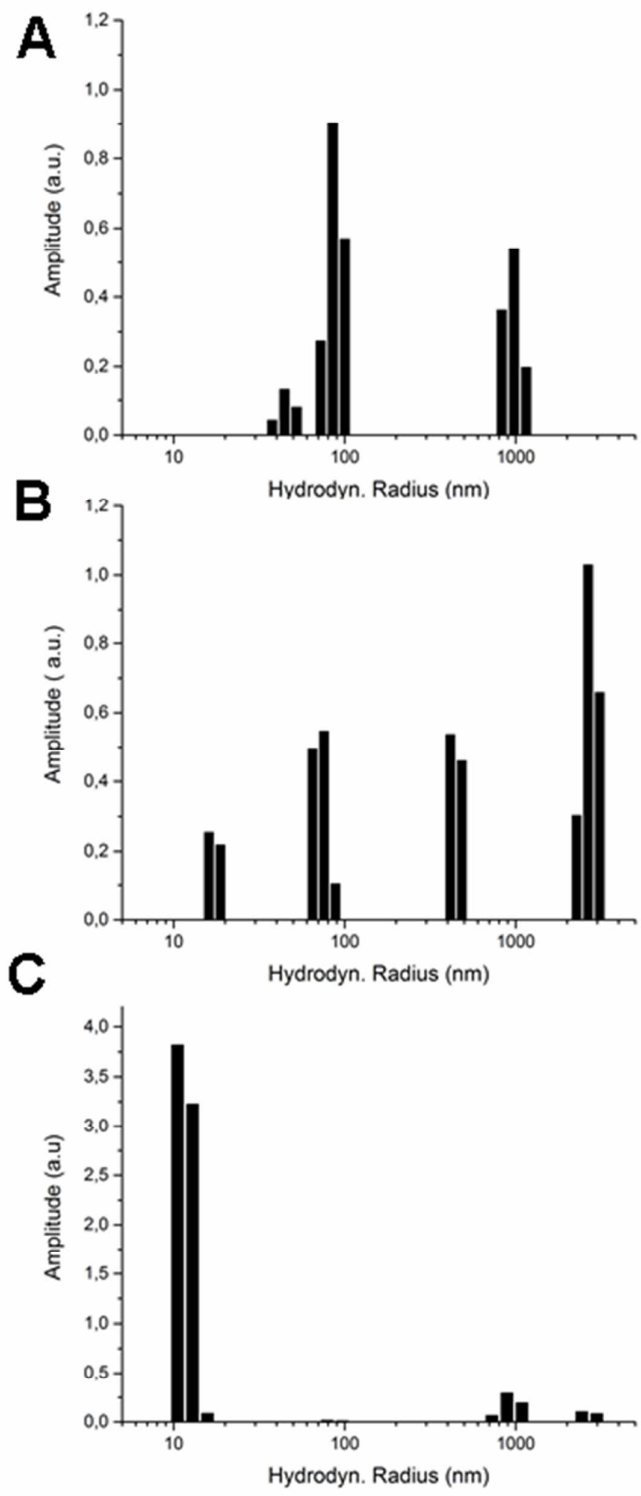

Figure 1. Size distributions of 33-mer in water at pH 7.0 at different concentrations: A) 125μM, B) 250 μM and C) 610μM. The distributions were obtained by inverse Laplace transformation of the field time correlation functions measured by dynamic light scattering. The mean radii value are summarized in Table 1.

View Article Online
DOI: 10.1039/C5SM01619C

At concentration below 125 μM, no significant scattering signal was detected with the used setup. The absence of aggregates below this concentration was confirmed by UV-Vis spectroscopy (see SI1).

Taking into account that all samples were filtered immediately prior measurement using a filter with a pore size of 220 nm, it was expected that only particles below this cut off appeared. However, different populations with larger sizes were detected, suggesting that small and larger particles are in equilibrium. The smallest particles are able to build up larger particles after filtration probably described by mass action law. [26] Upon increasing peptide concentration, we observed an increase of the relative intensity of the population below 100 nm and a decrease in the relative intensity of the others populations (hydrodynamic radii 100-1000 and ≥ 1000 nm). In addition, by increasing 33-mer concentration from 125 μM to 610 μM the hydrodynamic radii of the two populations below 100 nm, decreases from 46 ± 7 to 10 ± 3 nm and from 90 ± 9 to 75 ± 8 nm (Figure 1). These observations suggest that a dynamic interplay may exist between small and large particles. The larger particles probably act as new nucleation sites for smaller ones and limit the interaction between small ones. [26] Finally, after filtration the equilibration among species towards the higher order aggregates showed different kinetics of formation, in this case at 610 μM was the slowest. In this context, EM techniques showed that nanospheres, filaments and fibrils coexist at 610 μM. If we consider that fibrils and filaments are eliminated by filtration, the relative intensity of the smaller particles increases since the Rayleigh scattering intensity depends on R^6.

The change in the size distribution and intensity of the different populations observed has been previously described in the protein fibrillogenesis. In general, during this process, big aggregates can precipitate, fragment or even reorganize into new self-assembled structures thus changing the size distribution of the aggregates and their relative intensity. [27]

Finally, to test the contribution of electrostatic interactions in the aggregation of 33-mer peptide, a 250 μM solution of 33-mer peptide was prepared at a final ionic strength of

View Article Online
DOI: 10.1039/C5SM01619C

180 mM (10 mM of sodium citrate, sodium borate, sodium phosphate, and 150 mM of NaCl, pH 7).

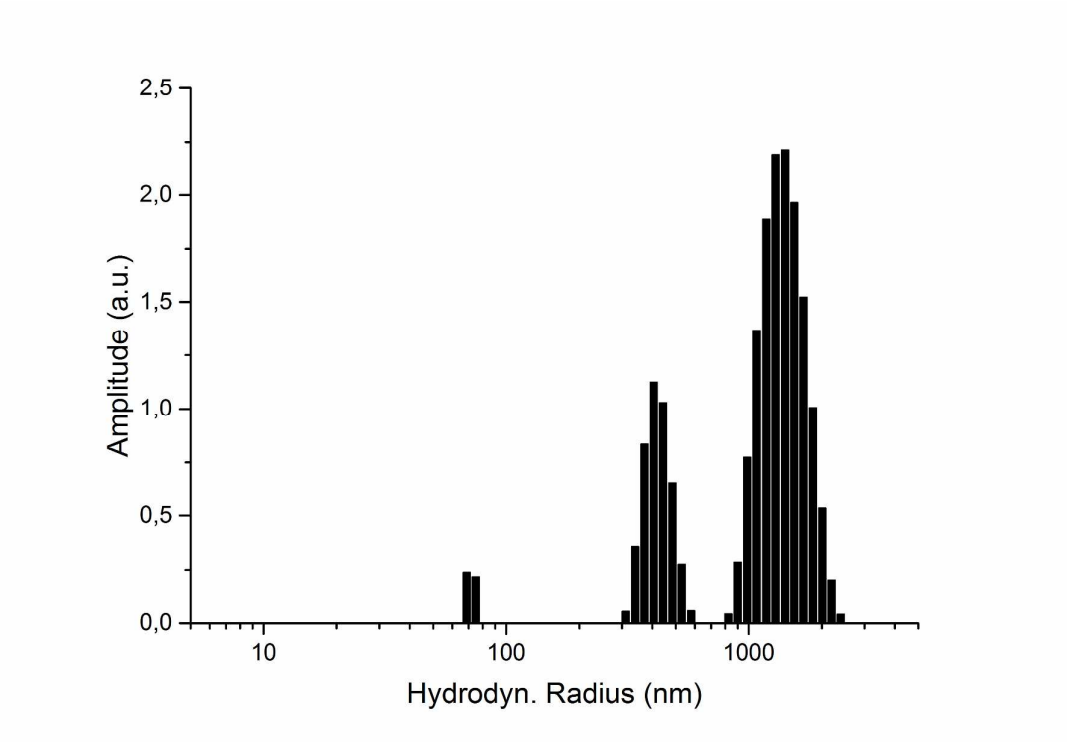

Figure 2. Size distribution of a 250 μM solution of 33-mer peptide in 10 mM of sodium citrate, sodium borate, sodium phosphate, and 150 mM of NaCl, pH 7. The distribution was obtained by inverse Laplace transformation of the field time correlation functions measured by dynamic light scattering. The mean radii value are summarized in Table 1.

This buffer was previously used to evaluate 33-mer structure in a biological context.[2, 8] Interestingly, the three aggregate categories persisted in the presence of salt and the hydrodynamic radius were comparable to those obtained in water, however the mean radii were higher than in pure water solution (compare Figure 2 and Figure 1B). These results suggest that the electrostatic interactions modify slightly the association among aggregates but they do not play a determining role in the self-organization behaviour of the 33-mer.

View Article Online
DOI: 10.1039/C5SM01619C

Concentration/Radius Mean Value	≤ 100 (nm)	100-1000 (nm)	≥ 1000 (nm)
125 µM in water	46 ± 7 90±9	962 ± 178	
250 µM in water	17±1 75±8	448±60	2784±866
250 µM in buffer	68± 9	424 ±87	1413 ± 452
610 µM in water	10±3	889±125	2437 ± 345

Table 1. Mean radii values of 33-mer gliadin peptide oligomers at different concentration in water at pH 7. 0 and in buffer solution (10 mM of sodium citrate, sodium borate, sodium phosphate, and 150 mM of NaCl) at pH 7.

At the molecular level, the forces involved in the 33-mer self-assembly process, can be correlated with the 33-mer primary structure. The 33-mer peptide, LQLQPF(PQPQLPY)$_3$PQPQPF, contains 65% of proline and glutamine, suggesting that hydrophobicity could be the driving force of the peptide's self-assembly. [28-30] Moreover, it is known that glutamine residues can interact via complementary hydrogen bonding, in addition to the aforementioned hydrophobic effect.[31-33] Previous molecular dynamics and partial electrostatics calculations carried out on the peptide, revealed a non-ionic amphiphilic nature. [8] Both characteristics would allow 33-mer to self-assemble into micelles which provides domains of high local protein concentration favouring oligomers formation. Similar Aβ micelles were proposed as precursors in the fibrillogenesis of amyloid β-protein. [34] The high polydispersity observed is consistent with the different quaternary structures sizes, previously detected by EM. [8] This polydispersity and dynamic behaviour among species has been described as a consequence of the metastability of self-assembling protein systems at physiological conditions [24], and reported for peptides such as β-amyloid [35, 36] and other self-organizing proteins such as αB- crystallin. [37]

Based on our results, we proposed that the 33-mer is able to form micelles that provide domains of high local protein concentration from which the oligomers are formed. The 33-mer micelles generated through still fluid associations are in equilibrium with

View Article Online
DOI: 10.1039/C5SM01619C

monomers as well as reversible smaller and larger complexes (Scheme 1). Upon increasing 33-mer concentration, the equilibrium among oligomers shifted towards filaments formation which are the only species eliminated from solution during filtration. Considering that previous CD experiments showed a conformational equilibrium between PPII and a β- like structure depending on its concentration, the hypothesis of structural transition and filament formation seems to be justified. [8] The existence of micelles and nano-structures can explain the observed fast diffusion of 33-mer through cell membranes. [7, 38]

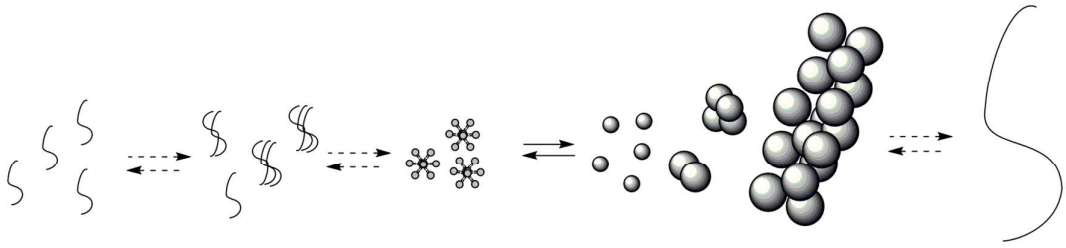

Scheme 1. Cartoon representing a hypothetic 33- mer peptide self-assembly process leading to the three self- assembled populations detected by DLS. We hypothesize that even if not detected by spectroscopic techniques dimers and/or other pre-micellar species could exist at concentrations lower than 125 μM.

Characterizing 33-mer aggregates onto bare mica by ex situ atomic force microscopy (AFM)

The main limitation to characterise the formed structures by EM was that at low concentrations only insufficient numbers or no particles were observed and no statistically significant results could be obtained for concentrations below 610 μM. On the other hand, AFM offers a unique opportunity to distinguish and characterize simultaneously multiple adsorbed species that vary strongly in size in a hydrated state and without chemical manipulation. In particular, ex-situ AFM, is a well-suited tool which has allowed to identify intermediates in the oligomerization pathways of different protein systems. [21, 39] In general, the process of a protein deposition and aggregation, which occurs when the solvent evaporates, eventually allows the precipitation of the

View Article Online
DOI: 10.1039/C5SM01619C

soluble species. This process results in complex architectures that are classified by physical properties, including fractal dimension, density and texture.[40-43] Here, negatively charged bare mica was selected as initial two dimensional substrate to evaluate 33-mer organisation by AFM mainly because of its low hydrophobicity (contact angle near 10°), [44] which is similar to the Formvar film used in our previous TEM experiments. [45] Moreover, it is well accepted that mica is a good substrate for mimicking the surface charge of cell membranes composed predominantly of anionic phospholipids, thus mimicking at least to some extent the 33-mer- membrane interaction *in vitro.* [46, 47]

33-mer gliadin peptide was deposited onto bare mica, at varying initial peptide concentrations. At 6 μM, discrete spherical structures and clusters were detected with an average height of 1.1 ± 0.5 nm (Figure 3).

View Article Online
DOI: 10.1039/C5SM01619C

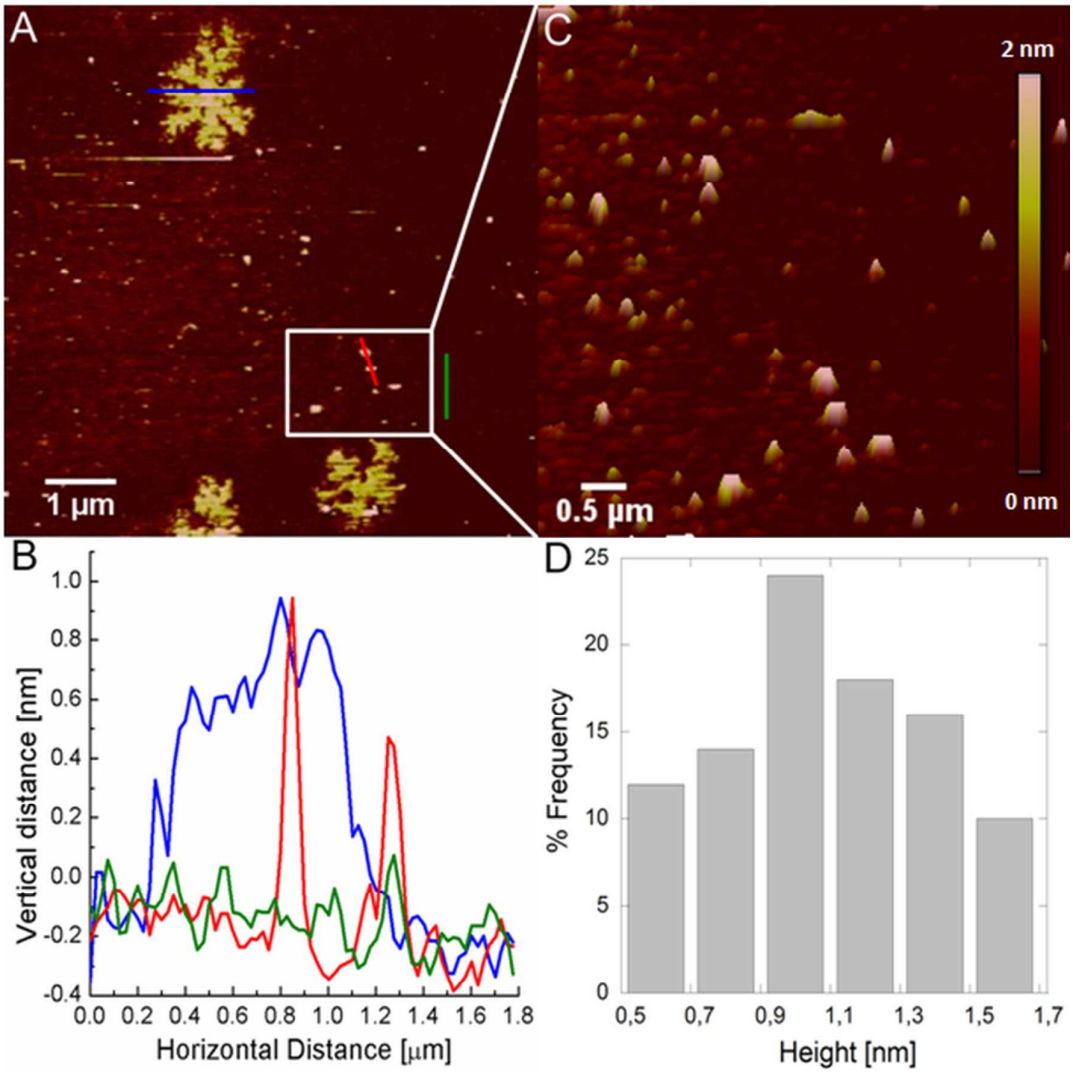

Figure 3. A). AFM image (topographic contact mode, 6 x 6 µm ^{2}) of 33-mer deposited on mica from a 6 µM aqueous solution at pH7. B) Cross section analysis of image A: the substrate (negatively charged bare mica) topography (green line) and the adsorbed peptide structures (red and blue lines). C) 3D image of the region marked as a square in image A, showing the discrete nanospherical structures. D) Height distribution of the total 33-mer structures detected in image A.

The average radii of discrete nanospheres are 6.40 ± 0.72 nm as calculated, using equations proposed by *Pietrasanta et. al.*[17] (see SI*)*. Considering that the isolated oligomers are spherical it was estimated that 156 molecules composed the smallest detected structure. [48, 49] The cluster architectures are similar to the fractal patterns that have been used to describe the diffusion-limited aggregation (DLA) of colloids and self-assembled peptides. [50, 51] The fractal nature of DLA architectures can be determined by

View Article Online
DOI: 10.1039/C5SM01619C

the fractal dimension parameter (D_f). The D_f found in modelling off-lattice DLA clusters is commonly 1.715 (DLA without dipolar interactions). Here, the D_f calculated by the box- counting procedure[21, 41] was 1.62 ± 0.02. It is known that in real systems, depletion effects may decrease D_f from the ideal value *of 1.71* to 1.40. [40, 52]

Considering that below 125 μM, no oligomers were detected by DLS, we can hypothesize that when the 33-mer solution was deposited on mica surface, the peptide primary structures were confined in a two-dimension environment. This increased surface concentration of 33-mer peptide could lead to the nucleation of the small spherical aggregates, detected at 6 μM. Under favourable conditions, some spherical particles could diffuse by Brownian motion on the substrate and form fractal clusters. In this context, individual particles can be considered as "seed" or nucleation sites in the self-assembly process.

Increasing 33-mer peptide concentration to 60 μM led to a greater surface coverage and different quaternary structures were detected (Figure 4). This observation suggests that solute concentration plays a major role in the 33-mer assembly process. This was previously proposed in other protein systems such as sericin and collagen.[21, 39]

Now, the spherical structures were distributed in an interconnected linear pattern and formed annular structures. The average height of the discrete spherical structures was 27.5 ± 6.0 nm; probably resulting from the coalescence of the previous smallest nanospherical structures detected at 6 μM (1.1 ± 0.5 nm). The absence of the smallest nanospheres, shows the ability of the oligomers to interact among each other, forming big spherical structures as shown in Fig. 4.

Additionally, two different types of planar structures appeared in minor proportions; one at 21.0 ± 5.4 nm and the second at 30.0 ± 5.6 nm average heights. The morphology of both planar structures is "sheet" like, reminiscent of linear filaments and plaques, respectively (Fig. 2 A and B: black and red lines). A careful analysis of the image

View Article Online
DOI: 10.1039/C5SM01619C

suggests a hierarchical organization of the system from isolated spherical structures to annular pore like structures and finally to the planar “sheet” like structures (Fig. 3C and D). The occurrence of different morphological structures during the 33-mer self-assembly on a mica surface suggests that the process is not only governed by the classical colloidal mechanism where particles undergo only coalescence.[53] Probably, some 33-mer oligomers through their intrinsic characteristics (size, and surface characteristics) would favour the formation of such new morphologies.

The D_f calculated at this concentration was 1.73 ± 0.02, this fractal dimension is consistent with scaling predictions [54], and explained by the presence of a polydisperse distribution of particles, providing additional nucleation sites for dendritic growth, increasing the D_f.

View Article Online
DOI: 10.1039/C5SM01619C

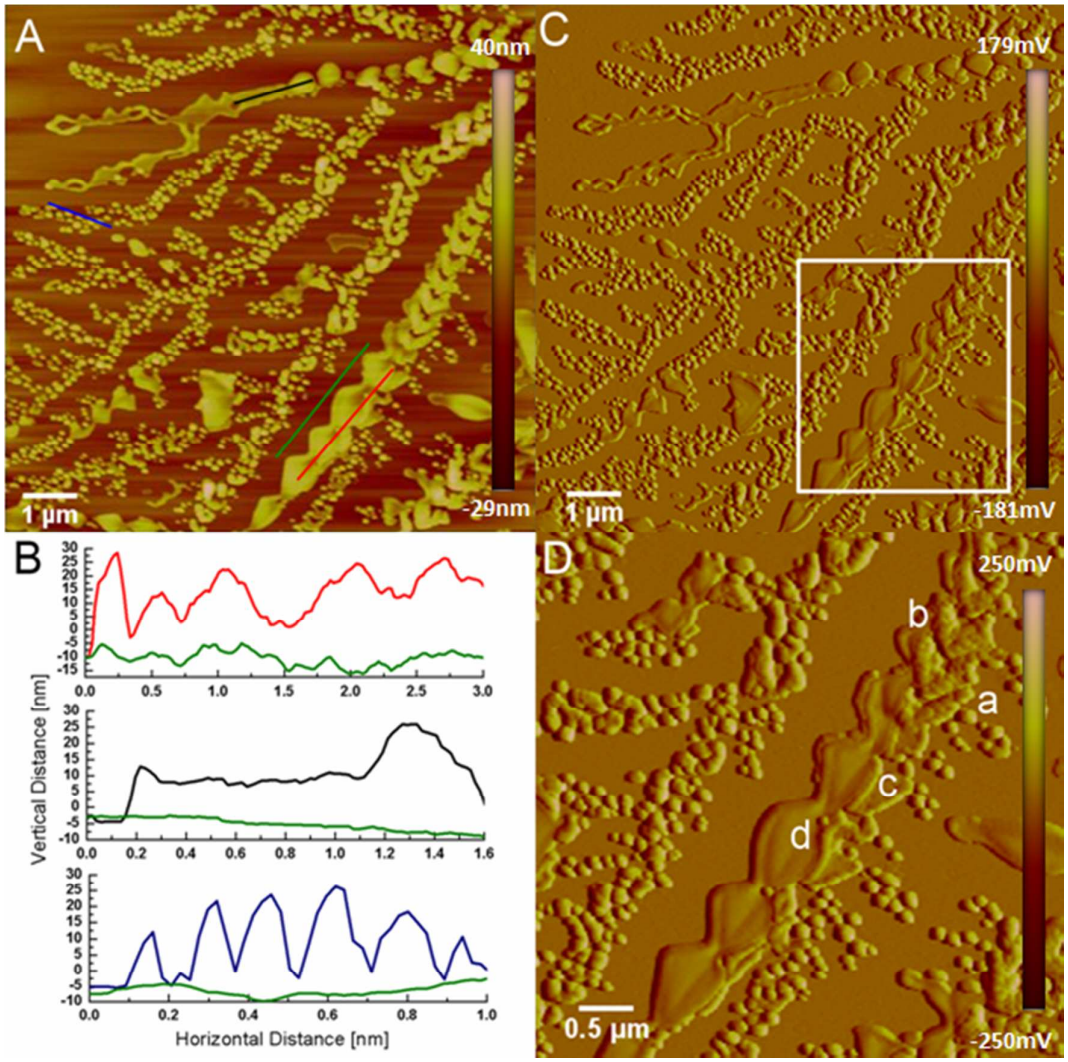

Figure 4. A) AFM image (topographic contact mode, 9.6 x 9.6 µm ^{2}) of 33-mer deposited on mica from a 60 µM aqueous solution at pH 7. Structures are shown with colored marks: plaques (red), filaments (black) and spheres (blue). B) Cross section analysis of image A: substrate topography (green line) and adsorbed peptide structures (red, blue and black lines). (Statistical distribution is available in supporting information S2). C) AFM image (deflection error) allows detailed observation of the 33-mer structures of image A. D) AFM image (deflection error, 4.8 x 4.8 µm ^{2}) of the section marked as square in image C, showing the hierarchical organization of 33-mer peptide from spherical structures (a), annular structures (b) to both planar structures: filaments (c) and plaques (d).

Increasing the concentration to 250 µM led to the detection of discrete spherical structures, linear and annular arrangement of them with average height around 14.0 ± 6.0 nm, 18.0 ± 2.0 nm and 28.0 ± 8.0 nm, respectively. At this concentration, the planar "sheet" like structures with a height in the range of 65 ±15 nm occupied most of the surface and seem to be the result of the coalescence of the spherical and annular

View Article Online
DOI: 10.1039/C5SM01619C

structures (Figure 5). Here, the D_f obtained was 1.73 ± 0.03 which is consistent with a DLA mechanism. In solution, DLS measurements showed the presence of structures with a polydisperse size distribution indicating that at 250 μM, the oligomerization process was already initiated in aqueous media. Although the observed final structures could be also modified by further interaction on surface, their size distribution is in the range of our DLS experiments at the same concentration. Again, it was not possible to detect the smallest nanospheres (1.1 ± 0.5 nm), showing the ability of the oligomers to interact among each other, forming the observed aggregate structures given in Figure 5.

View Article Online
DOI: 10.1039/C5SM01619C

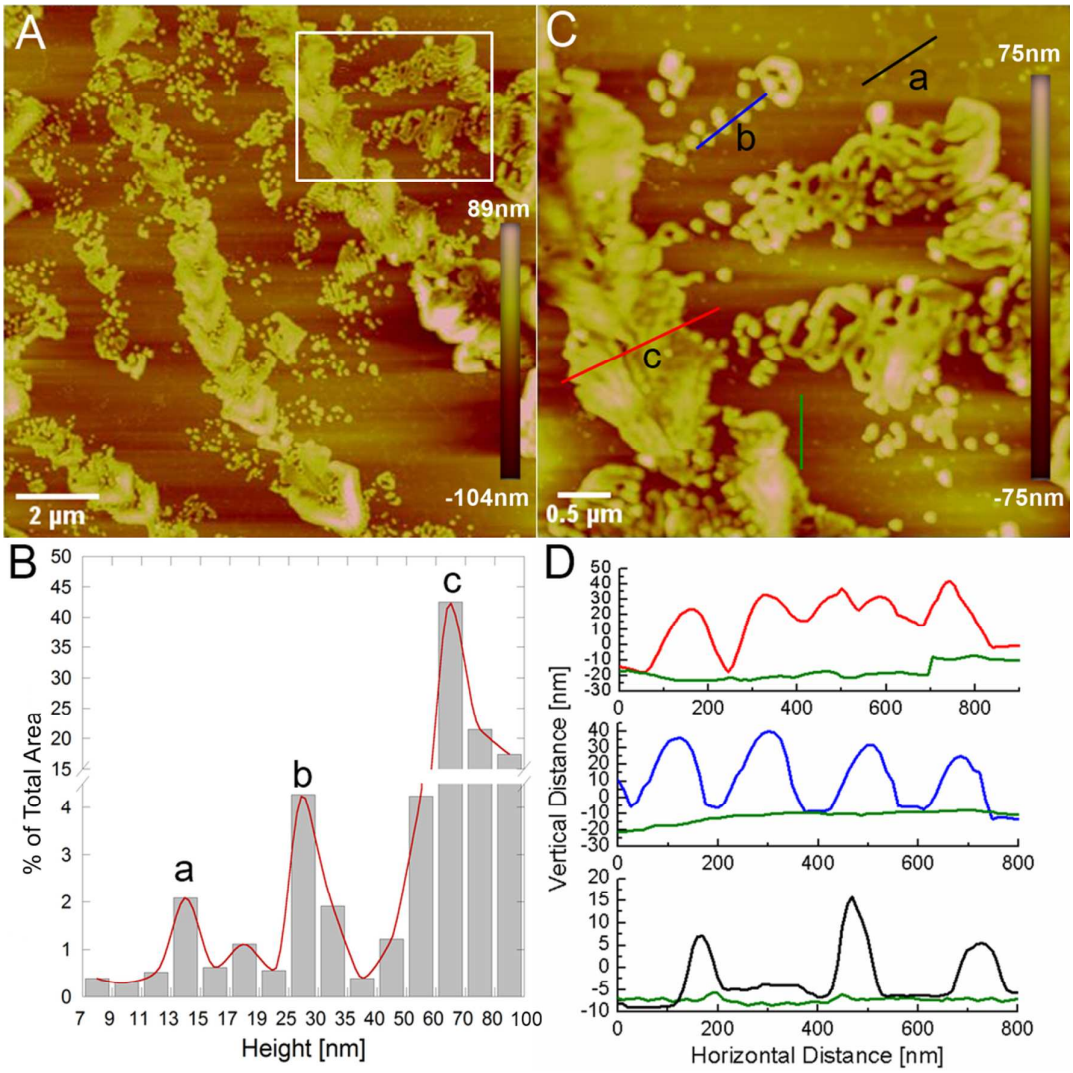

Figure 5. A) AFM image (topographic contact mode, 12.7 x 12.7 µm^2) of 33-mer deposited on mica from a 250 µM aqueous solution on at pH 7. B) Height distribution of the total 33-mer structures detected in image A: spherical structures (a), clusters of spherical structures (b) and planar structures (c). C) AFM image (topographic contact mode, 5 x 5 µm ^{2}) of the section marked as square in image A. Structures are shown with colored marks: plaques (red), clusters of spherical structures (blue) and isolated spherical structures (black). D) Cross section analysis of image C: the substrate (bare mica) topography (green line) and the adsorbed peptide structures (red, blue and black lines).

At 610 µM, deposition of 33-mer peptide assemblies on mica revealed that at this concentration, the system was mainly formed by linear interconnected filaments and plaques surrounded by spherical nanostructures (Figure 6).

The morphology of the 33-mer linear interconnected assemblies could be associated with soluble filaments (Figure 6) which were observed previously in other systems, like

View Article Online
DOI: 10.1039/C5SM01619C

in self-organized coiled-coil peptides [55] and in parallel beta-sheet structures of designed polypeptides. [56] The average height of the filaments was 35.8 ± 6.0 nm. The higher height detected (80.0 ± 20.0 nm) is consistent with plaques organized in a ladder fashion. As mentioned, filaments and plaques were surrounded by nanospherical structures of 5.1 ± 1.5 nm average height (see SI). In solution, previous CD [8] experiments detected that by increasing concentration, a structural transition towards a β structure occurred. In addition, the DLS experiments showed that upon increasing concentration, the relative intensity of the detected species changes. Considering the morphology of the aggregates on the surface, we hypothesize that increasing the peptide concentration, would favor one of the self-assembled structures formed in solution. Thus, the existence of filaments could explain the changes in the apparent hydrodynamic radii value and their relative size distribution depending on concentration.

On surface, the close proximity and reduction of degrees of freedom drive to the oligomers organization into a filament. Further lateral association between filaments could build up the detected plaques. The detection of filaments and spherical nanostructures simultaneously, in the absence of any intermediate particle (Fig. 6 and Fig. 7), implies that the filaments act as a new nucleation site for smaller particles, thus limiting the interaction between small particles. The fractal morphology was also observed by SEM on mica surface (see SI) being similar to those observed previously by EM. [8] This result is consistent with the presented DLS measurements at the same concentration (see above).

The calculated D_f decreases to 1.67 ± 0.04, which result from depletion effects as observed in the fractal assembly of coiled-coil peptides [55], silicatein nanospheres [57] and sericin. [21] This behaviour can be a consequence of the anisotropic geometry of the inter-peptide contacts that would favour adding the small oligomers along a preferred axis in the aggregate.

View Article Online
DOI: 10.1039/C5SM01619C

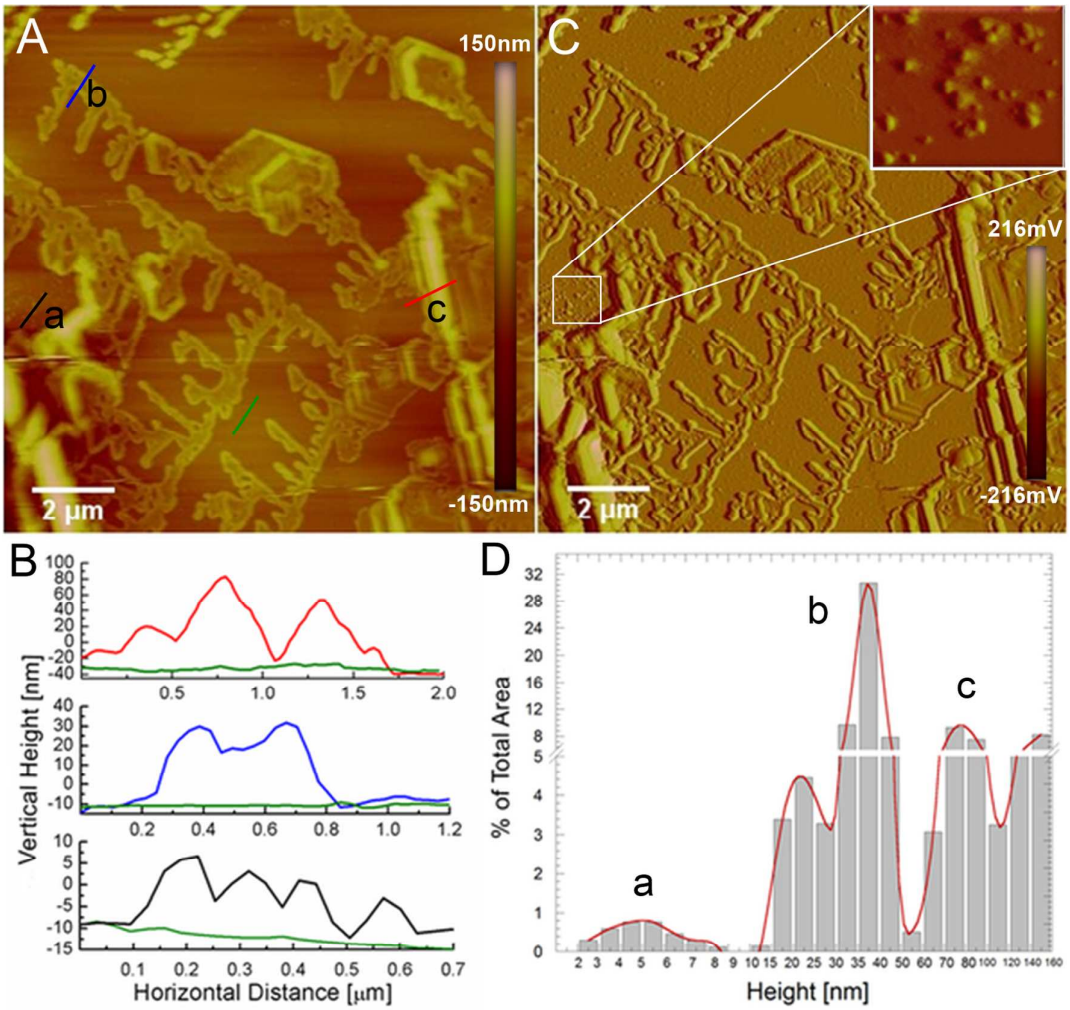

Figure 6. A) AFM image (topographic contact mode, 12.7 x 12.7 μm^2) of 33-mer deposited on mica from a 610 µM aqueous solution at pH 7. Structures are shown with colored marks: plaques (red), filaments (blue) and nanospherical structures (black). B) Cross section analysis of image A: the substrate topography (bare mica, green line) and the adsorbed peptide structures (red, blue and black lines). C) AFM image (deflection error) presenting a zoom of nanospherical structures D) Height distribution of the total 33-mer structures detected in image A: nanospherical structures (a), filaments (b) and plaques (c).

View Article Online
DOI: 10.1039/C5SM01619C

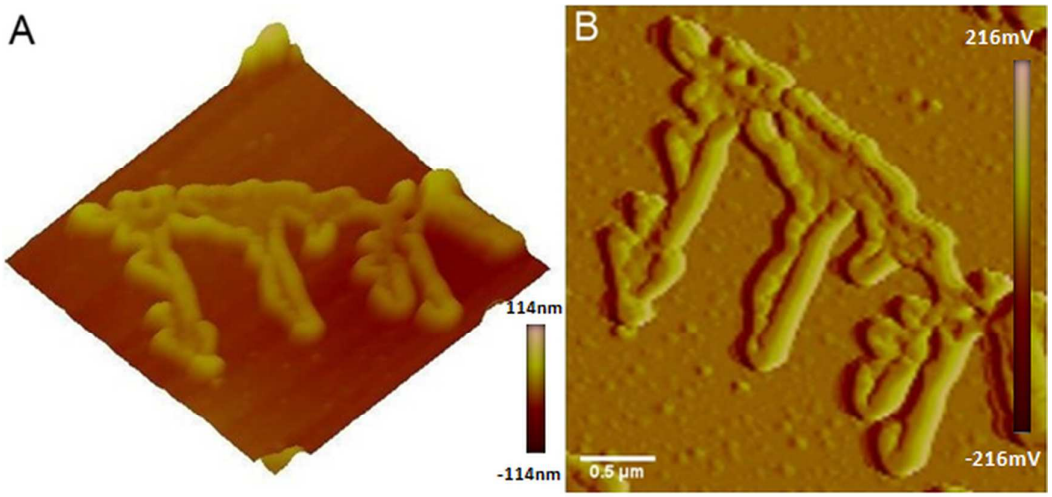

Figure 7. A) Three-dimensional AFM image (topographic contact mode, 3.2 x 3.2 μm^2) of 33-mer deposited on mica from a 610 µM aqueous solution at pH 7. B) AFM image (error deflection) showing the nanospherical structures in the background and the linear morphology of the filaments.

In summary, our AFM experiments revealed that the 33-mer peptide is able to self-assemble onto a bio-membrane mimetic surface like bare mica into not only nanospherical structures, but also linear and annular structures directed by DLA mechanism. Considering that by DLS on the filtered samples only particles were detected above the concentration of 125 µM, the structures observed at 6 – 60 µM could be the result of 33 mer self- assembly on mica surface. [58] Increasing the concentration up to 250 µM revealed the presence of similar structures. At 610 µM, the close proximity and reduction in degrees of freedom could drive oligomers condensation and organization into a filament, thus shifting the equilibrium towards filaments. Further lateral association between filaments could build up the detected plaques.

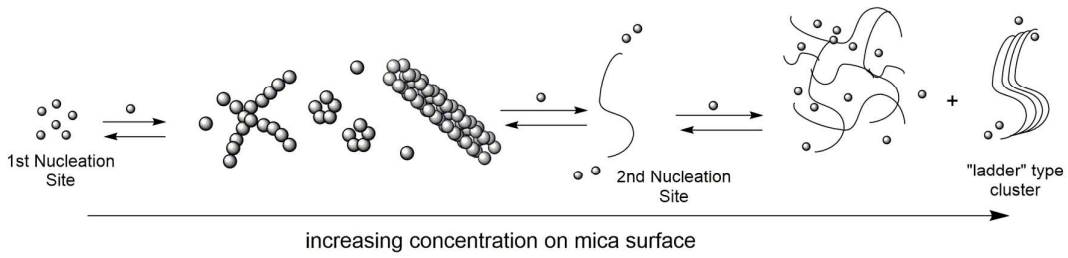

View Article Online
DOI: 10.1039/C5SM01619C

Scheme 2. Cartoon representing a summary of 33-mer self-assembly structures on increasing peptide concentration on mica surface.

The D_f values obtained at each concentration give a quantitative measure of the self-similarity of the structures and their increasing complexity with length scale. They are in close agreement with the theoretical value calculated for structures formed during a DLA process. [52] However, if we assume that 33-mer self-assembly on mica only is a colloidal like aggregation phenomenon governed by DLA, it may be expected that at increasing concentrations, the particles coalesce together to form indistinct films. On the mica surface, the 33-mer peptide generates fractal structures similar to colloids, which may be formed by the same process (DLA). However, the presence of different morphologies and finally the filaments suggests that the unique specific geometry of the 33-mer oligomers plays a crucial role in the subsequent condensation and organization of its fractal structures into the final filaments. This model of fractal DLA is an alternative mechanism of self-assembly of protein/peptides into filaments/fibrils and it was first proposed for silicatein [57] proteins and more recently for sericin. [21, 41]

ATR-FTIR experiments confirm secondary structure transition of 33-mer oligomers to β structure

A CD and nuclear magnetic resonance (NMR) study reported that a short sequence of the 33-mer (PQPQLPY) adopts a polyproline II helical (PPII) conformation. CD spectra recorded at different concentrations and environmental factors such as temperature and co-solvent interaction, showed that 33-mer peptide in aqueous media undergoes two concentration-dependent conformational transitions. [8] At low concentrations (6-197 μM), a transition from unordered to PPII structure occurs and is followed at concentrations above 197 μM with a second transition from PPII to a more folded one, probably a beta structure. It is well known that PPII conformation is always in equilibrium with other structures like β-turns, β-strands and unordered conformation, due to the close proximity of the respective dihedral angle. [59] Based on 33-mer primary

View Article Online
DOI: 10.1039/C5SM01619C

structure we hypothesised that a transition to a type II β turn took place in solution.[13] However, other β structures such as strands or sheets could be also involved. Here, taking advantage of the higher absorption coefficient in IR of the β-structure compared to CD [60], we investigated the nature of β-structure by ATR-FTIR. Experiments were carried out in water and after deuterium exchange, in the 50 to 610 μM concentration range.

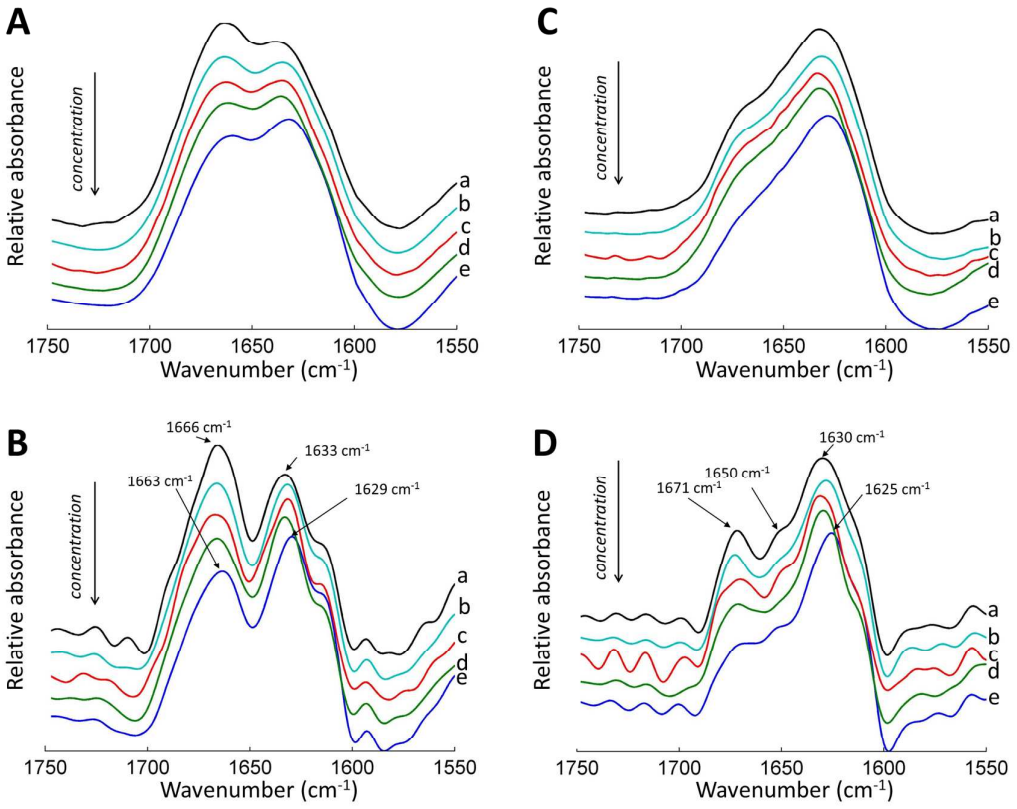

Figure 8. Normalized ATR-FTIR spectra of 33-mer peptide films in the Amide I region: (A) under nitrogen flux, or (C) $^{2}H_2O$-saturated nitrogen flux. Gliadin 33-mer concentrations were (a) 50 μM, (b) 100 μM, (c) 200 μM, (d) 300 μM, (e) 600 μM. A baseline drawn between the spectra data points at 1729 and 1575 cm^{-1} has been subtracted and spectra were rescaled to the same area below the amide I region (1729-1575 cm^{-1}). (B) and (D) are deconvoluted spectra of the same samples (A and C, respectively) with a resolution enhancement factor K = 2. All spectra were shifted for a better visualization.

View Article Online
DOI: 10.1039/C5SM01619C

ATR-FTIR spectra of 33-mer aggregates in the Amide I (representative of protein secondary structure) region revealed two main peaks (Fig. 8A). At 50 μM deconvolution of Amide I (Fig. 8B) showed two main peaks centred at 1666 and 1633 cm^{-1}. Increasing the concentration to 600 μM induced a red shift of both bands 1663 and 1629 cm^{-1}, respectively. Additionally, the area of the first peak (at 1630 cm^{-1}) is higher at 600 μM than at 50 μM (as evidenced by intensity ratios 1630/1660 cm^{-1} going from 0.82 to 1.18). These results are indicative of the existence of a conformational equilibrium among oligomers which depends on concentration and confirm our previous observation by CD.

The band around 1660 cm^{-1} is often representative of disordered conformations, but also potentially polyproline II structures. [61, 62] On the other hand, the band around 1630 cm^{-1} is assigned to a β-sheet structure. [62-64]

The increased peak intensity around 1630 cm^{-1} as compared to the peak around 1660 cm^{-1} as a function of concentration suggests that 33-mer peptide goes from a rather unordered state to a more folded state, enriched in β-structures. Furthermore, upon increasing concentration, a red-shift of the1633 cm^{-1} band to 1629 cm^{-1} was detected which could be correlated to inherent β-sheet properties like the assembly into longer sheets, longer β-strand formation as well as more planar sheet formation.[65, 66] The additional peak around 1695 cm^{-1}, characteristic for an antiparallel beta sheet structure[67], was not detected suggesting a parallel beta sheet structure, [65, 68-70] reminiscent of the fibril structure observed for protein aggregates associated to Alzheimer and Parkinson diseases. [71-75] After deuterium exchange (Fig. 8C), deconvolution of the Amide I band revealed a primary peak around 1633-1627 cm^{-1} usually associated with β-sheet structure. [62, 76] Disappearance of the first peak after deuteration confirms the disorder conformation. At 50 μM deconvolution of Amide I (Fig. 8D) showed three peaks centred in 1671, 1650 and 1630 cm^{-1}. Upon increasing the concentration to 600 μM, the latter peak shifts to 1625 cm^{-1}, and intensity ratios 1630/1671 cm^{-1} goes from 1.86 to 2.78, confirming a growing number of long β-strands

View Article Online
DOI: 10.1039/C5SM01619C

at elevated concentrations as compared to unordered structures. [69] These results are consistent with the morphology of the aggregates detected by AFM (compare Figure 3 to 6*)*. Considering that 33-mer is a proteolytic resistant peptide and is able to reach the intestinal lumen, the fact that it can adopt a superstructure with a β sheet parallel conformation at least *in vitro* led us to suggest this event as a potential molecular trigger which could break its tolerance and the development of the different pathologies.

Conclusion

Our findings demonstrated that 33-mer peptide in aqueous solution generates oligomeric aggregates coexisting with larger structures in the concentration range from 125 to 610 μM. Under our experimental conditions, 33-mer oligomers are in an equilibrium, which depends on peptide concentration, similar to micelle formation that is the classical example for association of colloids. Previous CD spectra recorded at the same concentrations showed that 33-mer oligomers exist in a conformational equilibrium between an extended PPII structure and a more folded β structure, associated with filaments formation.[8] Here it is hypothesised that the change in the hydrodynamic radii and relative intensity distribution observed by DLS could be associated to the mentioned structural transformation and filaments formation. Further cryo-TEM experiments are in progress in order to identify the morphology of 33-mer oligomers in solution. However, in general structural characterization of oligomers is, particularly challenging because of their often transient nature and, even more importantly, because of the variability of these species both in terms of size (from dimers to high-order multimers) and structure (from essentially random coil to a similar degree of β-sheet content to that observed in the fibrillar species). [77] It is therefore, one of our next goals to control the 33-mer oligomeric species formation in order to understand and obtain meaningful knowledge about their role in gliadin related disorders.

View Article Online
DOI: 10.1039/C5SM01619C

The self- assembly process of 33-mer on mica surface revealed that at low concentration (6-60 μM), 33-mer is able to self-assemble into nanospherical structures while an increase of the peptide concentration leads to the formation of other structures such as linear and annular arrays of spheres and planar "sheet" like structures such as filaments and plaques. Increasing the concentration to 610 μM led to formation of linear interconnected filaments and plaques surrounded by nanospherical structures. The self-assembly process in the whole concentration range could be qualitatively and quantitatively explained by considering diffusion limited aggregation (DLA) behaviour with D_f in the range of 1.62 ± 0.02 to 1.73 ± 0.03. The occurrence of fractal structures suggests that the 33-mer self-assembly process on mica follows the mechanism of fractal DLA.

Finally, ATR-FTIR experiments confirm the existence of oligomers in conformational equilibrium, which shifts to a more parallel β-sheet content by increasing 33-mer concentration. Both solution and surface experiments suggest that by increasing concentration the geometry of the inter-peptide contacts has a natural anisotropy that favours the interaction of nanospherical structures along a preferred axis of the filament, which is a typical nucleation mechanism of β sheet growth. The importance of parallel β sheet signature related to different protein derived diseases is well established,[78] and our research efforts are focused towards the isolation of the fibrils and evaluation of their structure by fiber X-ray diffraction. Meanwhile, the existence of 33-mer oligomers and their capability to build up a parallel β sheet is probably the first evidence that explains the simple hypothesis[79-81], that the persistence and accumulation of 33-mer *per se* in the intestinal lumen, might be a primary mechanism in celiac disease and possibly in other gliadin related disorders.

Acknowledgments

This work was supported by CONICET (National Scientific and Technical Research Council), ANCyPT (National Agency for Promotion of Science and Technology) and

View Article Online
DOI: 10.1039/C5SM01619C

UNS (Universidad Nacional del Sur) Argentinian Research grants, DAAD (German Academic Exchange Service), and by Alexander von Humboldt Foundation. M. G. H and L. A: B. are also grateful for their CONICET fellowship. V. I. D. and M. G. H thank Prof. R Salvarezza from INIFTA, Argentina for his support on AFM' s experiments, Prof. H Ritacco for first DLS's experiments, O. Wrede and Y. Hetler for DLS acquisition. V. I. D. thanks Prof. N. Sewald from Fakultät Chemie, Universität Bielefeld for his support to start this research project. T.H. gratefully acknowledges funding by the BMBF with in the framework of the project "05K13PB1 / 3DLS".

Competing financial interests

The authors declare no competing financial interests

References:

1. D. Bernardo, J. A. Garrote, L. Fernandez-Salazar, S. Riestra and E. Arranz, *Gut*, 2007, **56**, 889-890.
2. L. Shan, O. Molberg, I. Parrot, F. Hausch, F. Filiz, G. M. Gray, L. M. Sollid and C. Khosla, *Science*, 2002, **297**, 2275-2279.
3. K. E. Thomas, A. Sapone, A. Fasano and S. N. Vogel, *Journal of immunology*, 2006, **176**, 2512-2521.
4. A. Sapone, J. C. Bai, C. Ciacci, J. Dolinsek, P. H. Green, M. Hadjivassiliou, K. Kaukinen, K. Rostami, D. S. Sanders, M. Schumann, R. Ullrich, D. Villalta, U. Volta, C. Catassi and A. Fasano, *BMC medicine*, 2012, **10**, 13.
5. A. Rubio-Tapia, I. D. Hill, C. P. Kelly, A. H. Calderwood, J. A. Murray and G. American College of, *The American journal of gastroenterology*, 2013, **108**, 656-676; quiz 677.
6. M. Hadjivassiliou, C. A. Williamson and N. Woodroofe, *Trends in immunology*, 2004, **25**, 578-582.
7. M. Schumann, J. F. Richter, I. Wedell, V. Moos, M. Zimmermann-Kordmann, T. Schneider, S. Daum, M. Zeitz, M. Fromm and J. D. Schulzke, *Gut*, 2008, **57**, 747-754.
8. M. G. Herrera, F. Zamarreno, M. Costabel, H. Ritacco, A. Hutten, N. Sewald and V. I. Dodero, *Biopolymers*, 2014, **101**, 96-106.
9. P. Taboada, S. Barbosa, J. Juárez, M.-A. Meda and V. Mosquera, in *Proteins in Solution and at Interfaces*, John Wiley & Sons, Inc., 2013, pp. 233-282.
10. V. N. Uversky, J. Li and A. L. Fink, *The Journal of biological chemistry*, 2001, **276**, 10737-10744.
11. T. Town, V. Nikolic and J. Tan, *Journal of neuroinflammation*, 2005, **2**, 24.
12. C. M. Dobson, *Nature*, 2003, **426**, 884-890.

View Article Online
DOI: 10.1039/C5SM01619C

13. A. Nordskog, H. Egger, G. H. Findenegg, T. Hellweg, H. Schlaad, H. Von Berlepsch and C. Bottcher, *Physical review. E, Statistical, nonlinear, and soft matter physics*, 2003, **68**, 011406.
14. C. Urban and P. Schurtenberger, *Journal of Colloid and Interface Science*, 1998, **207**, 150-158.
15. S. W. Provencher, *Computer Physics Communications*, 1982, **27**, 229-242.
16. W. Fritzsche, A. Schaper and T. M. Jovin, *Chromosoma*, 1994, **103**, 231-236.
17. L. I. Pietrasanta, D. Thrower, W. Hsieh, S. Rao, O. Stemmann, J. Lechner, J. Carbon and H. Hansma, *Proceedings of the National Academy of Sciences of the United States of America*, 1999, **96**, 3757-3762.
18. C. A. Schneider, W. S. Rasband and K. W. Eliceiri, *Nat Meth*, 2012, **9**, 671-675.
19. E. Goormaghtigh, J.-M. Ruysschaert and V. Raussens, *Biophysical journal*, 2006, **90**, 2946-2957.
20. A. Lomakin, D. B. Teplow and G. B. Benedek, *Methods in molecular biology*, 2005, **299**, 153-174.
21. T. S. Khire, J. Kundu, S. C. Kundu and V. K. Yadavalli, *Soft Matter*, 2010, **6**, 2066-2071.
22. T. R. Serio, A. G. Cashikar, A. S. Kowal, G. J. Sawicki, J. J. Moslehi, L. Serpell, M. F. Arnsdorf and S. L. Lindquist, *Science*, 2000, **289**, 1317-1321.
23. C. Du, G. Falini, S. Fermani, C. Abbott and J. Moradian-Oldak, *Science*, 2005, **307**, 1450-1454.
24. D. B. Teplow, in *Methods in enzymology*, eds. K. Indu and W. Ronald, Academic Press, 2006, vol. Volume 413, pp. 20-33.
25. T. Hellweg, N. Henry-Toulmé, M. Chambon and D. Roux, *Colloids and Surfaces A: Physicochemical and Engineering Aspects*, 2000, **163**, 71-80.
26. Z.-J. Tan, X.-W. Zou, W.-B. Zhang and Z.-Z. Jin, *Physical Review E*, 1999, **60**, 6202-6205.
27. A. K. Buell, C. M. Dobson and T. P. Knowles, *Essays in biochemistry*, 2014, **56**, 11-39.
28. A. Morimoto, K. Irie, K. Murakami, H. Ohigashi, M. Shindo, M. Nagao, T. Shimizu and T. Shirasawa, *Biochemical and biophysical research communications*, 2002, **295**, 306-311.
29. M. J. Kogan, I. Dalcol, P. Gorostiza, C. Lopez-Iglesias, R. Pons, M. Pons, F. Sanz and E. Giralt, *Biophysical journal*, 2002, **83**, 1194-1204.
30. G. D. Darnell, J. Derryberry, J. W. Kurutz and S. C. Meredith, *Biophysical journal*, 2009, **97**, 2295-2305.
31. M. F. Perutz, *Current Opinion in Structural Biology*, 1996, **6**, 848-858.
32. R. Mishra and A. K. Thakur, *Organic & Biomolecular Chemistry*, 2015, **13**, 4155-4159.
33. M. F. Perutz, *Trends in Biochemical Sciences*, 1999, **24**, 58-63.
34. A. Lomakin, D. B. Teplow, D. A. Kirschner and G. B. Benedek, *Proceedings of the National Academy of Sciences*, 1997, **94**, 7942-7947.
35. D. M. Walsh, A. Lomakin, G. B. Benedek, M. M. Condron and D. B. Teplow, *The Journal of biological chemistry*, 1997, **272**, 22364-22372.
36. D. M. Walsh, D. M. Hartley, Y. Kusumoto, Y. Fezoui, M. M. Condron, A. Lomakin, G. B. Benedek, D. J. Selkoe and D. B. Teplow, *The Journal of biological chemistry*, 1999, **274**, 25945-25952.
37. Andrew J. Baldwin, H. Lioe, Gillian R. Hilton, Lindsay A. Baker, John L. Rubinstein, Lewis E. Kay and Justin L. P. Benesch, *Structure*, 2011, **19**, 1855-1863.
38. K. Mazumdar, X. Alvarez, J. T. Borda, J. Dufour, E. Martin, M. T. Bethune, C. Khosla and K. Sestak, *PloS one*, 2010, **5**, e10228.
39. V. K. Yadavalli, D. V. Svintradze and R. M. Pidaparti, *International Journal of Biological Macromolecules*, 2010, **46**, 458-464.
40. J.-F. Gouyet, in *Physics and Fractal Structures* ed. Springer, 1996.
41. N. E. Kurland, J. Kundu, S. Pal, S. C. Kundu and V. K. Yadavalli, *Soft Matter*, 2012, **8**, 4952-4959.
42. M. Tokuyama and K. Kawasaki, *Physics Letters A*, 1984, **100**, 337-340.

View Article Online
DOI: 10.1039/C5SM01619C

43. J. Choi, D. Crowdy and M. Z. Bazant, *EPL (Europhysics Letters)*, 2010, **91**, 46005.
44. H. Yang, S. Y. Fung, M. Pritzker and P. Chen, *PloS one*, 2007, **2**, e1325.
45. M. A. Hayat, *Principles and techniques of electron microscopy*, University Press: Cambridge, Cambridge, 2000.
46. J. D. Harper, S. S. Wong, C. M. Lieber and P. T. Lansbury, *Biochemistry*, 1999, **38**, 8972-8980.
47. T. T. Ding and J. D. Harper, in *Methods in enzymology*, ed. W. Ronald, Academic Press, 1999, vol. Volume 309, pp. 510-525.
48. S. W. Schneider, J. Larmer, R. M. Henderson and H. Oberleithner, *Pflugers Archiv : European journal of physiology*, 1998, **435**, 362-367.
49. C. Tanford, *Physical Chemistry of Macromolecules*, John Wiley and Sons Unites States of America, 1961.
50. T. A. Witten and L. M. Sander, *Physical Review B*, 1983, **27**, 5686-5697.
51. B. Mandelbrot, *The Fractal Geometry of Nature* W. H. Freeman and Company, New York, 1983.
52. P. Meakin, *Physical Review A*, 1983, **27**, 1495-1507.
53. P. Meakin, *Annual review of physical chemistry*, 1988, **39**, 237-267.
54. P. Ossadnik, C.-H. Lam and L. M. Sander, *Physical Review E*, 1994, **49**, R1788-R1791.
55. A. Lomander, W. Hwang and S. Zhang, *Nano Letters*, 2005, **5**, 1255-1260.
56. R. Sneer, M. J. Weygand, K. Kjaer, D. A. Tirrell and H. Rapaport, *ChemPhysChem*, 2004, **5**, 747-750.
57. M. M. Murr and D. E. Morse, *Proceedings of the National Academy of Sciences of the United States of America*, 2005, **102**, 11657-11662.
58. M. Zhu, P. O. Souillac, C. Ionescu-Zanetti, S. A. Carter and A. L. Fink, *Journal of Biological Chemistry*, 2002, **277**, 50914-50922.
59. B. Bochicchio and A. M. Tamburro, *Chirality*, 2002, **14**, 782-792.
60. E. Goormaghtigh, R. Gasper, A. Bénard, A. Goldsztein and V. Raussens, *Biochimica et Biophysica Acta (BBA) - Proteins and Proteomics*, 2009, **1794**, 1332-1343.
61. M. Martino, A. Bavoso, V. Guantieri, A. Coviello and A. M. Tamburro, *Journal of Molecular Structure*, 2000, **519**, 173-189.
62. A. M. Tamburro, A. Pepe, B. Bochicchio, D. Quaglino and I. P. Ronchetti, *The Journal of biological chemistry*, 2005, **280**, 2682-2690.
63. E. Goormaghtigh, V. Raussens and J. M. Ruysschaert, *Biochimica et biophysica acta*, 1999, **1422**, 105-185.
64. A. Barth, *Biochimica et Biophysica Acta (BBA) - Bioenergetics*, 2007, **1767**, 1073-1101.
65. Y. N. Chirgadze and N. A. Nevskaya, *Biopolymers*, 1976, **15**, 627-636.
66. J. Kubelka and T. A. Keiderling, *Journal of the American Chemical Society*, 2001, **123**, 6142-6150.
67. R. Sarroukh, E. Goormaghtigh, J. M. Ruysschaert and V. Raussens, *Biochimica et biophysica acta*, 2013, **1828**, 2328-2338.
68. W. H. Moore and S. Krimm, *Proceedings of the National Academy of Sciences of the United States of America*, 1975, **72**, 4933-4935.
69. Y. N. Chirgadze and N. A. Nevskaya, *Biopolymers*, 1976, **15**, 607-625.
70. E. Goormaghtigh, V. Cabiaux and J. M. Ruysschaert, *Sub-cellular biochemistry*, 1994, **23**, 329-362.
71. E. Cerf, R. Sarroukh, S. Tamamizu-Kato, L. Breydo, S. Derclaye, Y. F. Dufrene, V. Narayanaswami, E. Goormaghtigh, J. M. Ruysschaert and V. Raussens, *The Biochemical journal*, 2009, **421**, 415-423.
72. M. S. Celej, R. Sarroukh, E. Goormaghtigh, G. D. Fidelio, J. M. Ruysschaert and V. Raussens, *The Biochemical journal*, 2012, **443**, 719-726.
73. A. Sandberg, L. M. Luheshi, S. Sollvander, T. Pereira de Barros, B. Macao, T. P. Knowles, H. Biverstal, C. Lendel, F. Ekholm-Petterson, A. Dubnovitsky, L. Lannfelt, C. M. Dobson

View Article Online
DOI: 10.1039/C5SM01619C

and T. Hard, *Proceedings of the National Academy of Sciences of the United States of America*, 2010, **107**, 15595-15600.

74. S. Campioni, B. Mannini, M. Zampagni, A. Pensalfini, C. Parrini, E. Evangelisti, A. Relini, M. Stefani, C. M. Dobson, C. Cecchi and F. Chiti, *Nature chemical biology*, 2010, **6**, 140-147.
75. A. Gustot, V. Raussens, M. Dehousse, M. Dumoulin, C. E. Bryant, J. M. Ruysschaert and C. Lonez, *Cellular and molecular life sciences : CMLS*, 2013, **70**, 2999-3012.
76. M. Jackson and H. H. Mantsch, *Critical Reviews in Biochemistry and Molecular Biology*, 1995, **30**, 95-120.
77. S. W. Chen, S. Drakulic, E. Deas, M. Ouberai, F. A. Aprile, R. Arranz, S. Ness, C. Roodveldt, T. Guilliams, E. J. De-Genst, D. Klenerman, N. W. Wood, T. P. Knowles, C. Alfonso, G. Rivas, A. Y. Abramov, J. M. Valpuesta, C. M. Dobson and N. Cremades, *Proceedings of the National Academy of Sciences of the United States of America*, 2015, **112**, E1994-2003.
78. R. Tycko and R. B. Wickner, *Accounts of chemical research*, 2013, **46**, 1487-1496.
79. L. Tuckova, Z. Flegelova, H. Tlaskalova-Hogenova and Z. Zidek, *Journal of leukocyte biology*, 2000, **67**, 312-318.
80. L. Maiuri, C. Ciacci, I. Ricciardelli, L. Vacca, V. Raia, S. Auricchio, J. Picard, M. Osman, S. Quaratino and M. Londei, *Lancet*, 2003, **362**, 30-37.
81. J. L. Piper, G. M. Gray and C. Khosla, *The Journal of pharmacology and experimental therapeutics*, 2004, **311**, 213-219.

View Article Online
DOI: 10.1039/C5SM01619C

We report the spontaneous self-assembly of the 33-mer gliadin peptide, providing a better insight into oligomers morphology and secondary structure.